Hindawi
Shock and Vibration
Volume 2024, Article ID 1909530, 15 pages
https://doi.org/10.1155/2024/1909530

Research Article

An Investigation of the Acoustic Enclosure of an Air Conditioning Compressor Using Response Surface Analysis and Topological Rigidity Optimization

Hai-Feng Cao,[1] Cang-Jie Yang,[1] Ren-Lian Ma,[2] Shi-Wei Ni,[1] Zheng-Kai Song,[1] Xi Wang,[1] Yu-Xuan Chen,[1] and Chen-Xing Jiang[1]

[1]*Xiamen University, College of Energy, Xiamen, Fujian 361102, China*
[2]*GD Midea Air-Conditioning Equipment Co., Ltd., Foshan, Guangdong 528311, China*

Correspondence should be addressed to Xi Wang; wangxii512@xmu.edu.cn and Chen-Xing Jiang; jiangchx@xmu.edu.cn

Received 23 January 2024; Revised 29 March 2024; Accepted 27 April 2024; Published 9 May 2024

Academic Editor: Sébastien Besset

Copyright © 2024 Hai-Feng Cao et al. This is an open access article distributed under the Creative Commons Attribution License, which permits unrestricted use, distribution, and reproduction in any medium, provided the original work is properly cited.

A novel split-type air conditioning system is introduced to balance usability and portability. Unlike conventional split-type systems, where the compressor is typically placed outside, this system situates the compressor within the indoor unit, which may expose users to compressor noise. There are prominent peaks in the compressor noise spectrum, particularly at the compressor operating frequency and its harmonics, notably the second and third harmonics. The research presents a multilayered acoustic enclosure specifically designed for air conditioning compressors to address this issue without modifying the compressor or indoor unit casing. In order to get better sound insulation performance, a response surface methodology (RSM) is applied to optimize the thickness ratio, open area ratio, and open area height of the acoustic enclosure with predefined thickness. In addition, topological optimization is employed to strengthen weak areas of the acoustic enclosure. Then, experimental trials using the proposed acoustic enclosure are conducted in a semianechoic chamber. Results demonstrate significant reductions in noise levels, including 7.99 dB(A), 5.69 dB(A), and 5.19 dB(A) reductions in the fundamental frequency, second harmonic, and third harmonic noise of the compressor's operating frequency, respectively.

1. Introduction

The rapid advancement of technology leads to the pursuit of an enhanced quality of life. Since thermal problems influence indoor environmental quality most [1, 2], air conditioning units are continuously becoming the pivotal appliances that cater to human comfort. To optimize space utilization, some air conditioners include the compressor within the indoor unit. However, this design choice comes with an elevated noise level, which can affect the owner's experience.

In air conditioning noise reduction research, Choy et al. [3] focused on noise reduction in air conditioning duct systems and proposed a reinforced composite plate, highlighting the effectiveness of methods such as carbon fiber and aluminum foil reinforcement in enhancing the bending stiffness and transmission loss at low frequencies. Dandsena et al. [4] addressed the challenge of mitigating low-frequency noise produced by split-type air conditioner outdoor units using a tunable periodic array of solid scatters, named sonic crystal with hollow compartments and perforations, achieving a significant overall noise reduction of 7 dB. Mao et al. [5] investigated the noise characteristics of two-stage centrifugal compressors using a multilayer microperforated panel absorber designed to reduce tonal noise, particularly at the outlet pipe, and experimentally confirmed the noise reduction. Wu et al. [6] applied a combined approach of dynamic vibration absorption, sound absorption, and damping technologies to the outdoor unit of split-type air conditioners, achieving a 10 dB reduction in sound pressure levels.

These research objects are essentially air conditioners with traditional structures. However, for new indoor units, the scroll compressor, a crucial component in refrigeration and heat pump systems, stands out as the primary source of noise [7, 8]. The issue of low-frequency noise is of utmost severity. Due to engineering constraints on the compressor type, passive noise reduction measures are often employed to address such issues [9]. Damping materials are favored for their capacity to deliver outstanding sound insulation performance in passive control strategies [10, 11].

Wodtke et al. [12], through optimizing the combination of damping layers and concentrated mass, achieved a significant reduction in the low-frequency, wideband radiated sound power by reallocating unconstrained damping layers. Teng et al. [13] utilized the Ross–Kerwin–Unger (RKU) model to analyze the impact of design parameters on the vibration-damping characteristics of constrained damping structures. Li and Liang [14] analyzed the sound radiation characteristics of unconstrained damping plates under unit point excitation, utilizing response surface methodology (RSM) to determine the optimal plate thickness and material parameters to minimize the sound power. Axel et al. [15] introduced an integrated approach, assessing the presence or absence of damping plates from the perspective of noise transmission loss. Topological optimization is one of the common methods to improve the sound insulation performance of panels [16]. Zhang et al. [17] presented a study on the sensitivity analysis and topological optimization of attached damping layers to minimize sound radiation from vibrating shell structures under harmonic excitations. Wu et al. [18] focused on topological optimization techniques for enhancing the dynamic performance of constrained damping plates under the influence of frequency and temperature characteristics of damping materials.

In a confined space, composite panels are constrained by a limited thickness. Minimal effort and cost are required for reinforcing flat panels, resulting in an increased structural rigidity with minimal mass addition, thus enhancing the noise reduction performance [19]. Theoretical and experimental investigations of externally reinforced panels for industrial machinery noise control were conducted by Lee et al. [20], with the numerical results closely aligning with experimental findings. Cao et al. [21] theoretically investigated the acoustic properties of reinforced composite panels using first-order shear deformation theory, revealing a notable impact of reinforcement on the acoustic field. Shen et al. [22] addressed the acoustic transmission issues of periodically reinforced composite panels, by employing the spatial harmonic method to solve the acoustic vibration equation for periodic structures. They divided the acoustic response of the reinforced composite panel into four regions, providing insights into the acoustic design of orthogonally reinforced composite panels. Zhang et al. [23] performed multiobjective optimization on reinforced, high-sound-insulating, viscoelastic-damping composite panels. By optimizing the first sound insulation valley value, the damping layer insertion position, and the first modal loss factor, they improved the sound insulation performance of the composite panel under reinforced constraints. Zhu et al. [24] proposed an improved bidirectional evolutionary structural optimization (BESO) technique for topological optimization of a constrained layer damping treatment for the vibration suppression of an experimental rack backplane and demonstrated its effectiveness in achieving a reasonable layout with enhanced efficiency. Actually, different flow conditions could have an impact on sound wave propagation [25], which should be considered more in noise reduction.

There have been some research studies on noise reduction in traditional air conditioners, as well as theoretical research on sound insulation panels. When it comes to air conditioners including the compressor within the indoor unit, traditional noise reduction becomes inapplicable, while acoustic enclosure is a better choice. This paper addressed the low-frequency noise problem of a new split-type air conditioner by selecting steel plates and rubber as cost-effective base materials and establishing a reinforced acoustic enclosure within limited space constraints. The sound insulation performance is then optimized through response surface analysis and topological optimization.

The subsequent sections are organized as follows. Section 2 introduces the noise issues in the new split-type air conditioning system. Section 3 outlines the design and simulation optimization process of the acoustic enclosure. Section 4 presents experimental research validating the effectiveness of noise suppression. Finally, Section 5 provides conclusions.

2. The Noise Problem of the New Split Air Conditioner

Traditional air conditioners can be categorized structurally into split air conditioners and integrated air conditioners. The indoor unit of a split air conditioner typically includes a supply air fan, an evaporator, and an associated piping, while the outdoor unit comprises a condenser, a compressor, a heat dissipation fan, and a piping system. Integrated air conditioners, such as window units and portable air conditioners, feature components including the supply air fan, compressor, heat dissipation fan, condenser, and evaporator within a single structure.

Split air conditioners, due to constraints in coordinating the piping between indoor and outdoor units, are fixed in position after installation and challenging to move. Integrated air conditioners are easier to install and move, as they have a more compact structure. However, in terms of performance, split air conditioners, benefiting from the independent heating and cooling of indoor and outdoor units, outperform integrated air conditioners of the same power rating in terms of cooling and heating efficiency.

Therefore, as air conditioning applications become more widespread, innovative demands on air conditioner structures continue to emerge. To achieve the optimal balance between performance and portability, a novel structural design for split-type air conditioners is proposed in this work. The structural model of the indoor unit is depicted in Figure 1.

Figure 1 illustrates that this innovative split air conditioner indoor unit includes a supply air fan, an evaporator,

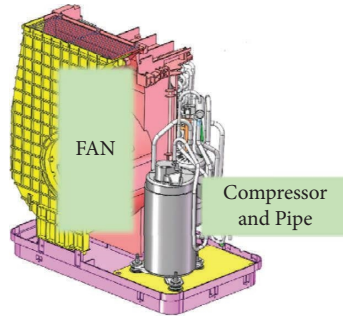

Figure 1: A structural model of the new air conditioner indoor unit.

and the associated piping system. Wheels can be installed at the bottom for easy mobility. The outdoor unit, on the other hand, consists only of a condenser and heat dissipation fan, making it structurally simple. The connection between the outdoor and indoor units comprises the inlet and outlet pipes of the condenser and the power lines for the heat dissipation fan, allowing for easier arrangement. This air conditioning structure is newly proposed by our cooperative manufacturer.

However, due to the installation of the compressor inside the indoor unit, this new split air conditioner requires a more focused consideration of noise levels compared to traditional split-type air conditioners. The air conditioner employs a scroll compressor, and its noise primarily consists of high-frequency electromagnetic noise from the motor, low-frequency mechanical noise from the compression rotor, as well as valve plate sounds and fluid noise associated with the opening and closing of internal valves. The low-frequency mechanical noise from the compressor is mainly generated by the rotational frequency and the second-harmonic and third-harmonic excitations, generally occurring below 500 Hz [26].

Figure 2 shows the survey results of an air conditioning manufacturer. The main source of the data is the manufacturer's regular inquiries with the air conditioning users and after-sales feedback. As depicted in Figure 2, the low-frequency noise produced by the compressor is a crucial factor affecting user perception. This is especially true when the compressor is located indoors, where complaints about low-frequency compressor noise are more prevalent. Investigations of the noise attenuation characteristics reveal that, at the same distance, low-frequency noise attenuates less than high-frequency noise [27]. Therefore, researchers should give special consideration to the low-frequency noise generated by the indoor unit compressor in this particular structural design of air conditioners.

In the development of air conditioning products, once the compressor model is decided, it cannot be modified, and the inherent noise characteristics of the compressor unit become fixed accordingly. Controlling the noise source of the compressor proves challenging under these circumstances. Therefore, this study focuses on optimizing the acoustic performance of the acoustic enclosure for the indoor unit's specific noise characteristics.

3. Design and Simulation

3.1. Acoustic Enclosure-Type Design. Due to the predetermined spatial requirements of the compressor and its piping system during the product design phase, the shape and size of the acoustic enclosure must align with the spatial constraints of the compressor and the outer casing of the air conditioner indoor unit. Based on measurements from an actual air conditioner model, it was determined that the compressor and its piping system occupy approximately $180 \times 270 \times 420$ mm of space. In addition, due to limitations in component spacing, designing an all-encompassing acoustic enclosure, by excluding the bottom surface of the compressor, requires maintaining a thickness of around 1 mm. As depicted in Figure 3, the shape of the acoustic enclosure is derived from the actual structural configuration of the compressor unit.

Damping is a physical effect that impedes the relative motion of objects and converts the energy of motion into other forms of energy, and it is also a key factor in determining the acoustic transmission performance of a structure [28]. Consequently, due to the favorable mechanical properties of damping material, employing a composite-constrained damping structure yields better acoustic performance than a single-layer panel. Research has confirmed the effectiveness of this method in noise reduction [29]. To meet practical engineering cost requirements, the base and constrained layer use steel as a material, while rubber serves as the damping layer. The schematic multilayer constrained damping structure is shown in Figure 4(a), and the actual diagram is shown in Figure 4(b). Simultaneously, considering the layout requirements for the compressor piping, specific openings of equal height need to be placed on the two designated faces of the acoustic enclosure, as depicted in Figure 5.

This paper employs RSM to explore the influence of the open area ratio, open area height, and damping layer thickness ratio on the acoustic performance of the acoustic enclosure. The effects of these three parameters on the results are not independent. It is difficult to obtain the optimal effect if the influence of each parameter on the acoustic enclosure effect is explored separately. The effect of the acoustic enclosure is determined by the interaction of the three parameters. Hence, we have to use a method to represent the interaction between parameters. The purpose of RSM is to

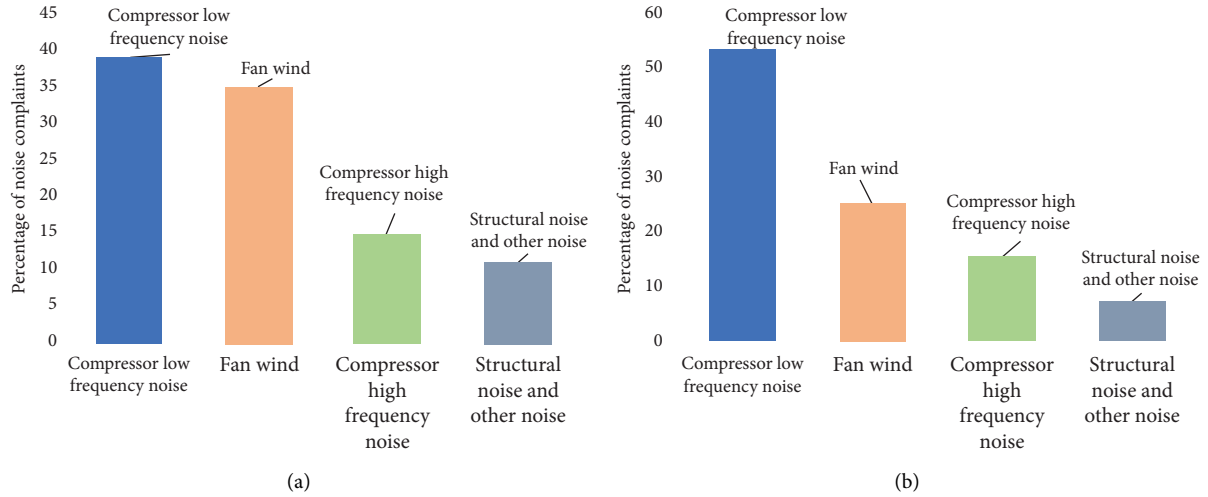

Figure 2: Air conditioning manufacturer's market research on air conditioning noise. (a) The percentage of noise complaints for traditional split air conditioners. (b) The percentage of noise complaints for traditional one-piece air conditioners.

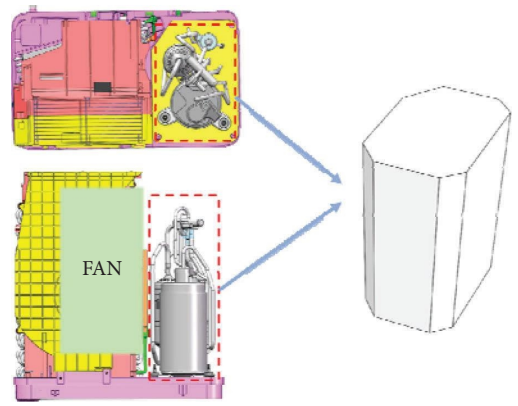

Figure 3: Determination of the acoustic enclosure shape.

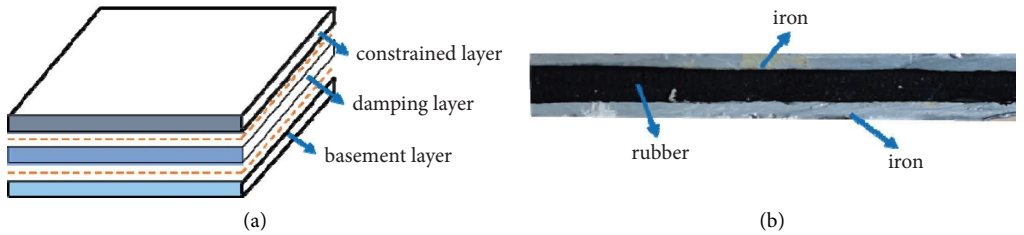

Figure 4: Multilayer constrained damping structure. (a) Schematic diagram. (b) Actual diagram.

approximate the mapping relationship between a finite number of design variables and the output response value through an explicit mathematical polynomial. The core idea behind RSM lies in using a limited number of experimental trials to fit this explicit mathematical polynomial.

The fundamental concept of RSM [30] involves expanding variables based on the Taylor series to construct a polynomial. Different forms of polynomials, such as linear, quadratic, cubic, and higher-order polynomials, are chosen based on the number and levels of design variables. A linear polynomial is generally chosen to express the mathematical relationship when there are few design variables and no interactions among them. When there are interactions among the design variables, a higher-order polynomial is selected for fitting. Considering the trade-off between computational accuracy and cost, this paper adopts a quadratic polynomial to fit the response surface, expressed as follows:

$$y = c_0 + \sum_{i=1}^{m} c_i x_i + \sum_{i=m+1}^{2m} c_{ii} x_{i-m}^2 + \sum_{i=1}^{m-1} \sum_{j=i+1}^{m} c_{ij} x_i x_j, \quad (1)$$

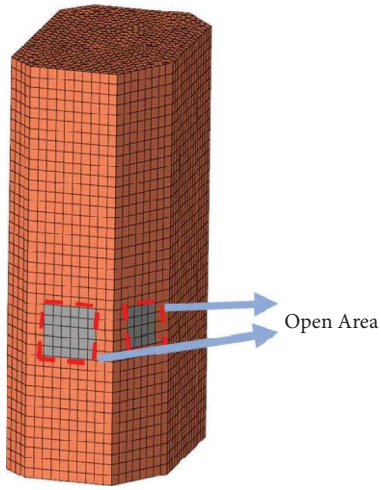

Figure 5: A schematic diagram of the acoustic enclosure apertures.

where x represents the design variables, y is the output response value, m is the number of design variables, c_0 is the constant term, c_i is the coefficient of the linear term, c_{ii} is the coefficient of the quadratic term, and c_{ij} is the coefficient of the interaction term.

The design variables, namely, the open area ratio (α), open area height (β), and damping layer thickness ratio (γ), are defined as follows. The open area ratio (α) represents the ratio of the open area of the piping to the surface area, with a specified range of 0–0.2. The open area height (β) is the ratio of the open distance to the height of the acoustic enclosure, assuming the sound source is at the middle height, with a range of 0–0.5. The damping layer thickness ratio (γ) is the ratio of the thickness of the damping layer to the sum of the thicknesses on both sides, with a total thickness of 1 mm and a range of 0.05–0.35. When γ is below 0.05, there is insufficient machining precision. Conversely, if γ exceeds 0.35, the metal plates of the acoustic enclosure become excessively thin, resulting in inadequate support.

In this paper, the response surface output values are assessed using the following two noise indicators:

(a) Low-frequency noise level (AVE1): the average of the root-mean-square (RMS) values of the 0–100 Hz spectrum noise at a distance of 1 m from the acoustic enclosure, measured in dB(A).

(b) Broadband noise level (AVE2): the average of the root-mean-square (RMS) values of the 0–1500 Hz spectrum noise at a distance of 1 m from the acoustic enclosure, measured in dB(A).

Therefore, in this paper, the expression to be evaluated is as follows:

$$AVE1 = c_0 + c_1\alpha + c_2\beta + c_3\gamma - c_{11}\alpha^2 - c_{22}\beta^2 - c_{33}\gamma^2 + c_{12}\alpha\beta + c_{13}\alpha\gamma + c_{23}\beta\gamma, \tag{2}$$

$$AVE2 = c_0' + c_1'\alpha + c_2'\beta + c_3'\gamma - c_{11}'\alpha^2 - c_{22}'\beta^2 - c_{33}'\gamma^2 + c_{12}'\alpha\beta + c_{13}'\alpha\gamma + c_{23}'\beta\gamma. \tag{3}$$

Establishing a high-precision and efficient response surface model generally requires a rational experimental design. The selected sample points should sufficiently reflect the characteristics of the entire experimental design space, making it a crucial aspect of constructing the response surface model. Commonly used methods for sample selection include central composite design (CCD) [31], Latin hypercube sampling design [32], orthogonal experimental design [33], and Box–Behnken experimental design [34]. Considering the complexity of the mapping relationship between design variables and output response values, the central composite design method is adopted in this paper to construct the sample space. The experimental design yields the experimental program as shown in Table 1.

The noise indicators are calculated using the frequency domain indirect boundary element method.

The boundary element method (BEM), as compared to the finite element method (FEM), avoids the 3D meshing issues associated with thin-walled structures, thereby enhancing the quality of the computational mesh [35]. Derived from the BEM, the indirect boundary element method (IBEM) significantly reduces the computational complexity [36]. In the IBEM, Helmholtz integral equations are simultaneously established on both sides of the boundary. The subtraction of these two integral equations yields the calculation of the sound pressure at any observation point, as shown in equation (2).

$$\begin{aligned} p(r_p) &= \iint_s \left[G(r_p, r_q)\left(\frac{\partial p(r_{q1})}{\partial n} - \frac{\partial p(r_{q2})}{\partial n} \right) - \frac{\partial G(r_p, r_q)}{\partial n_q}\left(p(r_{q1}) - p(r_{q2}) \right) \right] dS(r_q) \\ &= \iint_s \left[G(r_p, r_q)\sigma(r_q) - \frac{\partial G(r_p, r_q)}{\partial n_q}\mu(r_q) \right] dS(r_q), \end{aligned} \tag{4}$$

where $\sigma(r_q)$ represents the gradient of the normal pressure on both sides of the surface and $\mu(r_q)$ is the acoustic pressure difference across the surface, and when one side has an acoustic pressure $p(r_{q2}) = 0$, $\mu(r_q) = p(r_{q1})$. By defining the observation points on the boundary with the position vector r_q, the relationship between the boundary conditions and the unknown primary variables can be established as

Table 1: The experimental program.

Number	α	β	γ
1	0.2	0.5	0.05
2	0.1	0.25	0.2
3	0.1	0.25	0.05
4	0.2	0	0.05
5	0	0	0.05
6	0.1	0	0.2
7	0.1	0.25	0.35
8	0.1	0.5	0.2
9	0	0.5	0.35
10	0	0	0.35
11	0	0.25	0.2
12	0.2	0	0.35
13	0.2	0.5	0.35
14	0	0.5	0.05
15	0.2	0.25	0.2

$$\frac{\partial p(r_p)}{\partial n_p} = \iint_s \left(\frac{\partial G(r_p, r_q)}{\partial n_p} \sigma(r_q) - \frac{\partial^2 G(r_p, r_q)}{\partial n_p \partial n_q} \mu(r_q) \right) dS = -i\rho\omega v(r_p), \tag{5}$$

where $v(r_q)$ represents the velocity at the surface r_q of the boundary model, ρ is the density of the medium, and ω is the angular frequency of the medium's motion. The unknown primary variables on the surface of the boundary element model can be expressed in terms of the primary unknown variables at the nodes of the model and their shape functions. Utilizing the variational principle, a general form can be derived as

$$[A]\{x\} = \{F_a\}, \tag{6}$$

where $[A]$ represents a symmetric matrix determined by the geometry of the boundary and the properties of the medium. It is obtained through integration of the Green's function and its partial derivatives. $\{x\}$ denotes the primary unknown variables on the surface of the boundary element model and $\{F_a\}$ is the excitation force function vector. Obtaining the primary variables through equation (6), the sound pressure at any point can then be calculated by using equation (4).

The air conditioning compressor is a rotary compressor, and its sound source characteristics comply with the alternating expansion and contraction characteristics of a dipole sound source [37]. Therefore, a dipole sound source is employed to simulate the compressor for simulation analysis, with the sound source positioned in the middle of the acoustic enclosure. The total thickness of the three-layer material of the acoustic enclosure is 1 mm, and multilayer shell elements are used to simulate the constrained damping structure during grid meshing. The material parameters for steel and rubber are set as shown in Table 2:

In this study, LMS Virtual.Lab was used for acoustic computation. This is shown in Figure 6. Before acoustic computation, structural models with different parameter combinations are established and modal calculation is performed to obtain modal information. The modal information is imported into Virtual.Lab to use the IBEM calculation module. Meanwhile, the acoustic mesh model is established and imported into the calculation module. According to the abovementioned analysis, the sound source is a dipole sound source, and the propagation medium is air. In order to simulate the installation base of the actual sound shield, the baffle is set in the simulation. The computational field is 2 m × 2 m square, the center of which is the geometric center of the acoustic enclosure.

Noise calculations were performed for each test scenario. According to the test standard of the air conditioning manufacturer, the noise assessment point is located one meter outside the compressor. So the field point one meter away from the sound source is selected as the noise response point in the simulation. The results were extracted as shown in Table 3.

The computational results of each test scenario were compiled and RSM was performed. The regression equation for the response output values is shown in the following equation:

Table 2: Material property parameters.

Material	Density (kg/m^3)	Elastic modulus (MPa)	Poisson's ratio
Steel	7850	210000	0.3
Rubber	1200	100	0.47

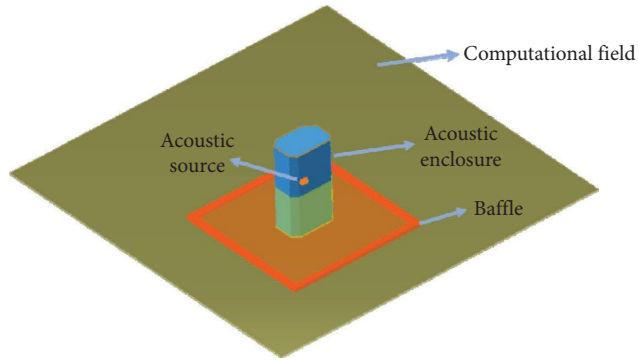

Figure 6: The setup for acoustic computing.

Table 3: Noise calculation results for each test program.

Number	α	β	γ	AVE1 (dB(A))	AVE2 (dB(A))
1	0.2	0.5	0.05	32.25	85.73
2	0.1	0.25	0.2	29.34	84.40
3	0.1	0.25	0.05	29.34	84.20
4	0.2	0	0.05	27.79	83.68
5	0	0	0.05	26.77	81.52
6	0.1	0	0.2	27.34	83.01
7	0.1	0.25	0.35	29.39	84.40
8	0.1	0.5	0.2	30.94	85.71
9	0	0.5	0.35	26.70	81.77
10	0	0	0.35	26.70	81.77
11	0	0.25	0.2	26.83	82.01
12	0.2	0	0.35	27.81	83.34
13	0.2	0.5	0.35	32.29	85.66
14	0	0.5	0.05	26.77	81.52
15	0.2	0.25	0.2	30.76	85.14

$$AVE1 = 26.55 + 18.21\alpha + 2.81\beta + 0.85\gamma - 63.00\alpha^2 - 4.54\beta^2 - 2.64\gamma^2 + 44.68\alpha\beta + 1.69\alpha\gamma + 0.05\beta\gamma, \quad (7)$$

$$AVE2 = 81.18 + 29.75\alpha + 1.70\beta + 4.47\gamma - 93.8\alpha^2 - 2.46\beta^2 - 9.40\gamma^2 + 21.87\alpha\beta - 7.56\alpha\gamma + 0.90\beta\gamma. \quad (8)$$

The interaction effects of the open area ratio α, the open area height β, and the damping layer thickness ratio γ on the low-frequency noise level are illustrated in Figure 7. In Figure 7(a), the central condition is set to be an open area ratio α of 0.1, and Figure 7 depicts the interaction between the open area height β and the damping layer thickness ratio γ. Figure 7(b), with a central condition of the open area height β being equal to 0.25, demonstrates the interaction between the open area ratio α and the damping layer thickness ratio γ on the low-frequency noise level. Finally, Figure 7(c), with a damping layer thickness ratio γ of 0.2, shows the interaction between the open area height β and the open area ratio α for the low-frequency noise level.

From Figure 7, it can be observed that the thickness ratio of the damping layer has a relatively small impact on the low-frequency noise level. In contrast, the open area ratio α and open area height β exhibit significant effects, showing a generally linear increase within the considered range. Notably, the open area ratio α has a greater impact than the open area height β on the low-frequency noise level, and the proximity of the open area to the sound source position amplifies the influence of the open area ratio α.

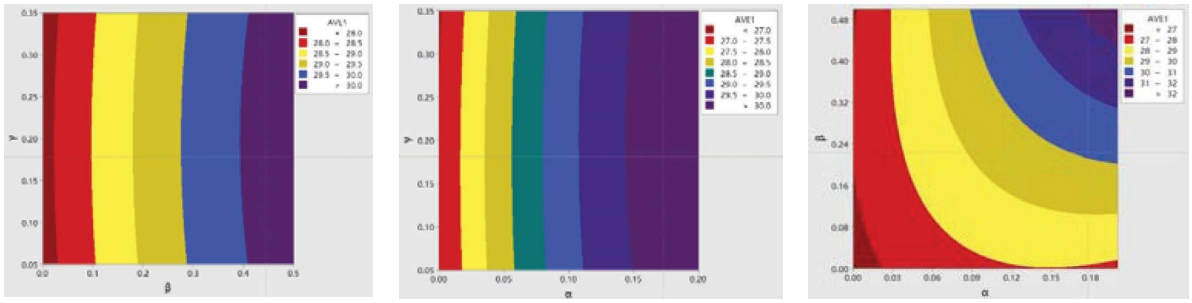

(a) (b) (c)

Figure 7: Interactions between variables on AVE1. (a) Interaction between β and γ. (b) Interaction between α and γ. (c) Interaction between α and β.

Figure 8(a) explores the interactive effects of the open area height β and the thickness ratio of the damping layer γ on the broadband noise level, considering an open area ratio α of 0.1 as the central condition. Figure 8(b), with an open area height β of 0.25 as the central condition, investigates the interactive effects of the open area ratio α and the thickness ratio of the damping layer γ on the broadband noise level. Figure 8(c), using a thickness ratio of the damping layer γ of 0.2 as the central condition, examines the interactive effects of the open area height β and open area ratio α on the broadband noise level.

It is observed from Figure 8 that the impact of the open area ratio α on the broadband noise level starts to plateau after 0.1. The open area height β maintains a linear positive correlation with the broadband noise level, while the thickness ratio of the damping layer γ peaks around 0.2 in the broadband noise level.

Considering practical manufacturing challenges, the final selection is an open area ratio α of 0.05, a damping layer thickness of 0.05 mm, and both base and constraint layer steel plate thicknesses of 0.5 mm, with the open area located at the bottom of the wall.

3.2. Rigidity Optimization of the Acoustic Enclosure. Due to the limited space inside the air conditioner, the total thickness of the designed acoustic enclosure in the previous section was only 1.05 mm. This may result in insufficient overall rigidity, leading to issues such as low-frequency resonance and deformation. Therefore, it is necessary to consider enhancing the rigidity of the acoustic enclosure.

First, to identify the weaker areas of the acoustic enclosure, modal analysis is conducted to observe the modal shape distribution. Modal analysis is a common method in the field of structural dynamics used to study the dynamic characteristics of structures [38]. Modes represent the inherent vibrational characteristics of mechanical structures, each with specific natural frequencies and mode shapes. Modal analysis reveals the characteristics of the main modes within a certain frequency range where the structure is susceptible to external or internal vibrations.

The original finite element model of the acoustic enclosure is shown in Figure 5, and the block Lanczos modal extraction method is employed to obtain the modal analysis results. Since the compressor operates at a frequency of 50 Hz, particular attention is given to the low-order overall deformation modes of the acoustic enclosure. The modal frequencies and shapes are presented in Table 4.

Analysis of the modal calculation results reveals that the original acoustic enclosure exhibits distinct low-order resonance modes around the compressor operating frequency. Additionally, the modal shapes indicate that maximum displacements occur on the two broader faces of the original enclosure. Therefore, considering previous research findings, this study explores the reinforcement of the broader faces of the original enclosure to enhance its overall rigidity.

In choosing a reinforcement approach, this study employs topological optimization using the solid isotropic microstructures with penalization (SIMP) method. The model can be described as follows:

$$\begin{cases} \min f(x) = U^T K U = \sum_i u_i^T k_e u_i, \\ \text{s.t. } KU = P, \\ V(x) - V(0) = \sum_i^N V_i(x_i) - V_0 \le 0, \\ 0 \le x_i \le 1, \quad i = 1, 2, \cdots, N, \end{cases} \tag{9}$$

where P is the load vector, U is the displacement vector, K is the overall stiffness matrix, k_e is the elemental stiffness matrix, x is the density matrix, composed of microelement densities x_i from the topological optimization, where the total number of elements is denoted as N, and V_0 represents the upper limit constraint on the structural volume. Solving the optimization model yields the density matrix under the volume constraint.

In this method, the "element density" of each unit in the design space is treated as a design variable. The element density is associated with the material parameters of the structure and takes continuous values between 0 and 1. After optimization, an element density of 1 (or close to 1) indicates that the material at that unit location is crucial and should be retained, while an element density of 0 (or close to 0) implies that the material at that unit location is less important and can be considered for removal, thereby achieving efficient material utilization.

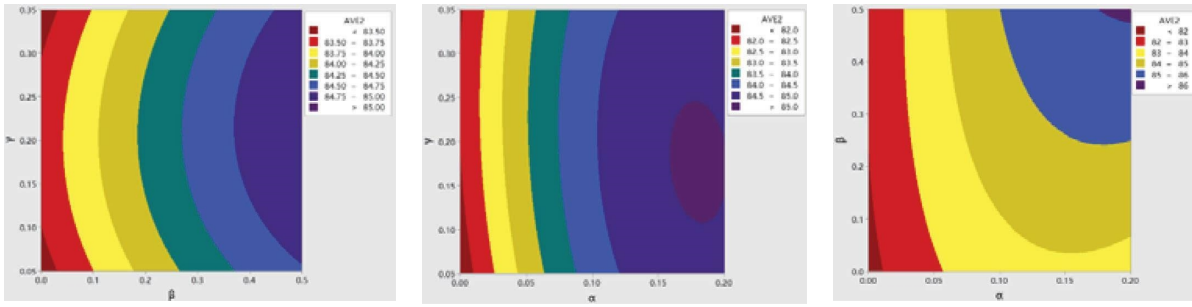

(a) (b) (c)

Figure 8: Interaction between variables on AVE2. (a) Interaction between β and γ. (b) Interaction between α and γ. (c) Interaction between α and β.

Table 4: The original acoustic enclosure low-order modal information.

Modal frequency (Hz)	Displacement vector plots	Displacement cloud plots
47.93	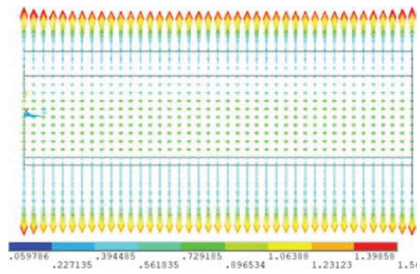	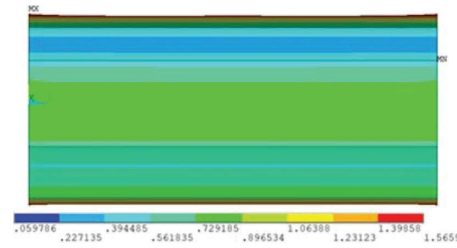
54.05	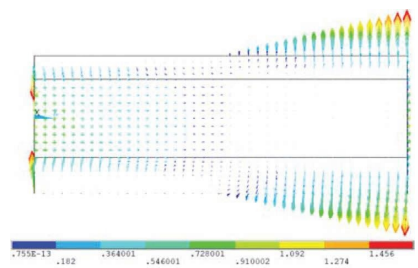	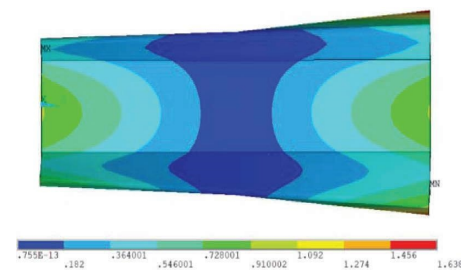

For the topological optimization settings, as shown in Figure 9, the optimization plane is represented by a green surface. Geometric constraints require fixing the lower part of the acoustic enclosure. The objective constraint aims to minimize the overall flexibility of the optimization plane, corresponding to maximizing stiffness. The load is applied in the middle of the optimization plane to simulate the impact of the compressor's acoustic source on the acoustic enclosure. The results of the topological optimization are presented in Figure 10.

Analysis of the topological optimization results reveals that retaining the red area in Figure 10 achieves the condition of minimal volume while maximizing the rigidity. Therefore, to enhance the original acoustic enclosure's rigidity, reinforcement within the red area is chosen for optimal effectiveness.

The topological optimization results exhibit extensions at all four corners, with the purple points in Figure 11 requiring particular attention. These results suggest that diagonal reinforcement has a more significant impact on the rigidity of the acoustic enclosure than other forms of reinforcement. Therefore, considering cost and manufacturing constraints, as depicted in the model on the right side of Figure 11, we opt for the stamping of 0.3 mm stainless steel "X"-shaped ribs on the two wide surfaces of the original acoustic enclosure. This approach yields a more effective enhancement in rigidity.

To better illustrate the enhanced rigidity effect of the reinforcement, this study utilizes the block Lanczos modal extraction method to compute the modal information for the reinforced acoustic enclosure. The modal results corresponding to the same order as the original acoustic enclosure are analyzed, and the results are presented in Table 5.

Upon analysis, it is evident that, for the same order and compared with the original acoustic enclosure, the acoustic enclosure with added stainless steel "X"-shaped ribs experiences an increase in modal frequencies from 47.928 Hz to 54.053 Hz to 117.62 Hz and 143.04 Hz, respectively. The overall maximum displacement decreases from 1.57 to 1.64

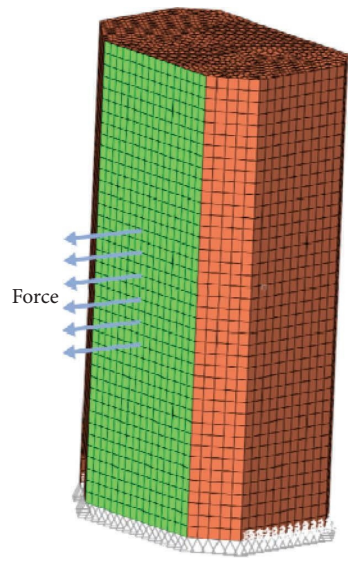

Figure 9: Topological optimization: optimization plane and excitation schematic.

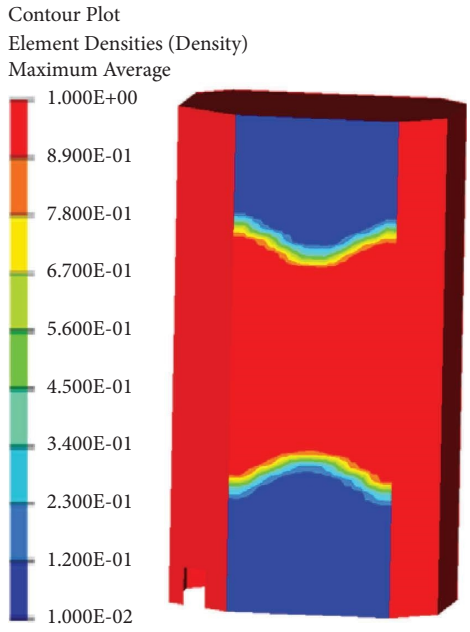

Figure 10: Topological optimization results.

to 1.01 and 1.54, with an improvement in the significant displacement deformation on the two wide sides. In summary, adding stainless steel "*X*"-shaped ribs effectively enhances the acoustic enclosure's rigidity.

4. Experiment

To validate the effectiveness of the research findings described above, experimental investigations were conducted under three sets of operational conditions.

The testing was performed in a semianechoic chamber with an ambient temperature of 42°C and the air conditioner was set to operate at 16°C. The compressor frequency was locked at 50 Hz using a controller. To minimize the influence of the indoor unit fan on noise testing, the fan speed was set to its minimum, reducing airflow noise. Noise signals were captured at a distance of 1 m from the compressor side of the indoor unit using a PCB microphone. The collected data were processed and analyzed using a data acquisition system, yielding the final results of the noise tests. A schematic diagram is presented in Figure 12, and the experimental equipment is detailed in Table 6.

The background noise of the semianechoic chamber was tested and the results are shown in Figure 13.

Analyzing the background noise test results reveals that the noise spectrum from 0 to 1500 Hz is generally below 0 dB(A), having no significant error impact on the experimental results. Subsequent experiments were then

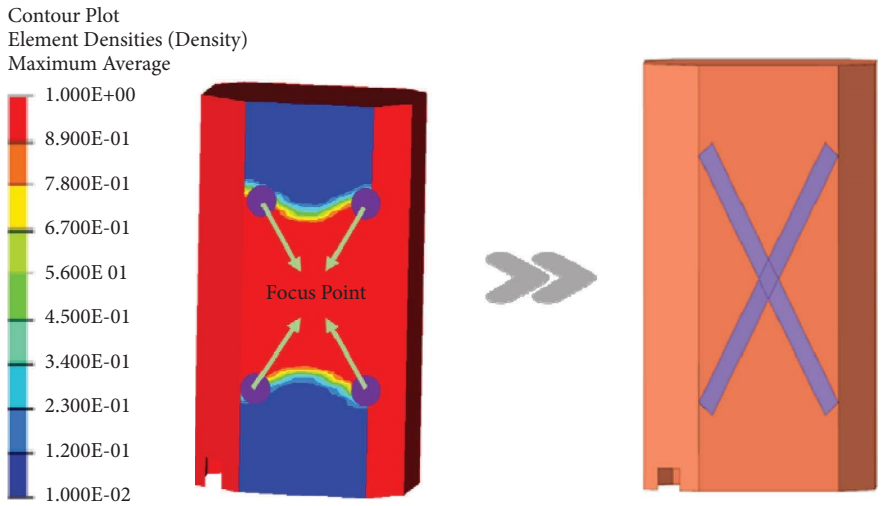

Figure 11: Topological optimization analysis.

Table 5: Low-order modal information of the acoustic enclosure after rigidity enhancement.

Modal frequency (Hz)	Displacement vector plots	Displacement cloud plots
117.62	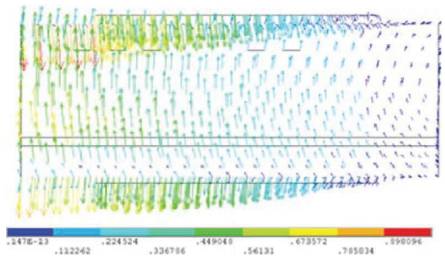	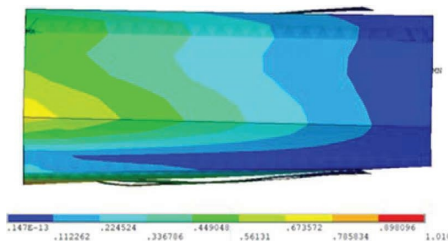
143.04	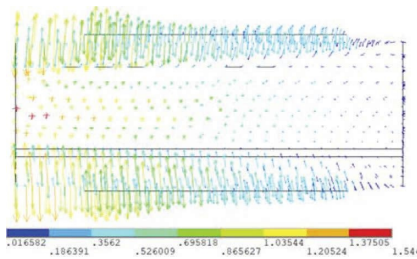	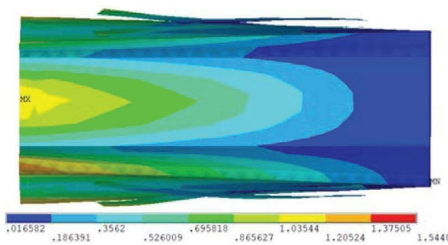

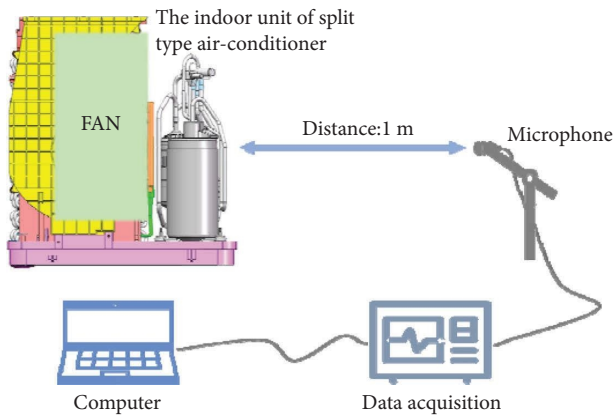

Figure 12: A schematic diagram of the experiment.

Table 6: The experimental equipment.

Equipment name	Type	Number	Unit
Data acquisition instrument	LMS SCADAS Mobile SCM2E05	1	Set
Microphone	PCB 378B02	1	Set
Test notebook	ThinkPad T490	1	Set

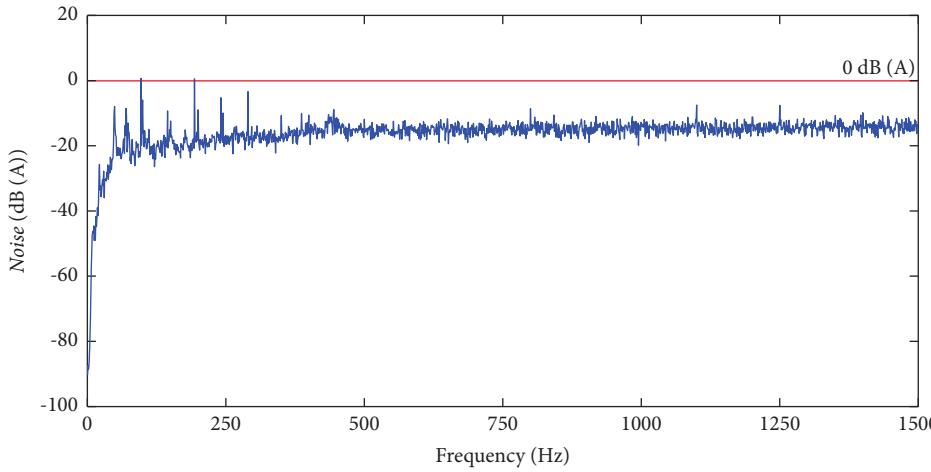

Figure 13: The test environment background noise.

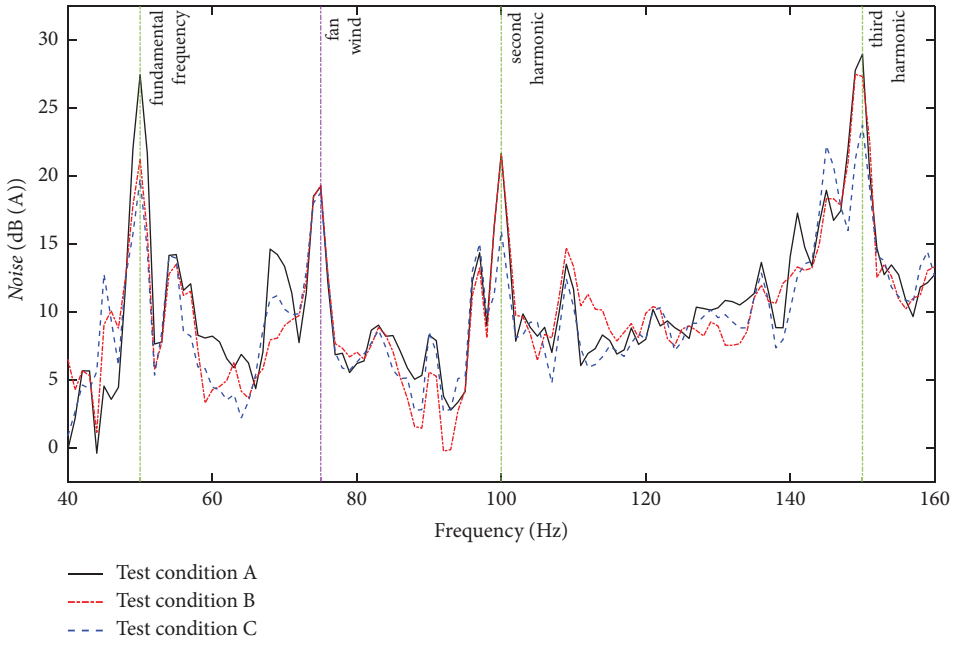

Figure 14: Test noise comparison.

conducted. The acoustic enclosure tests were conducted under three sets of conditions as follows:

(1) Test condition A: a new split air conditioner unit with no enclosure cover on the compressor.

(2) Test condition B: a new split air conditioner unit with an RSM-optimized enclosure mounted on the compressor.

(3) Test condition C: a new split air conditioner unit with an enclosure strengthened for rigidity mounted on the compressor.

The air conditioning compressor operates at a frequency of 50 Hz, with a focus on its fundamental frequency, second harmonic, and third harmonic. The results obtained under each condition are compared in Figure 14.

Table 7: A comparison of the test noise indicators.

Indicator	Test condition A	Test condition B	Test condition C
Fundamental frequency noise (dB(A))	27.45	21.24	19.79
Fundamental frequency loss (dB(A))	—	6.21	7.99
Second harmonic noise (dB(A))	21.66	21.62	15.97
Second harmonic loss (dB(A))	—	0.04	5.69
Third harmonic noise (dB(A))	28.95	27.32	23.76
Third harmonic loss (dB(A))	—	1.63	5.19

By analyzing the peaks in Figure 14, the main frequencies observed are 50 Hz, 75 Hz, 100 Hz, and 150 Hz. The 75 Hz noise is attributed to the indoor fan and cannot be reduced by the acoustic enclosure on the compressor. The 50 Hz, 100 Hz, and 150 Hz noise correspond to the fundamental frequency, second harmonic, and third harmonic of the compressor's operation, which are reduced to varying degrees with the installation of the acoustic enclosure. To provide a clearer analysis of the sound insulation effectiveness, a comparison of the compressor's fundamental and harmonic noise values is presented in Table 7.

From the analysis in Table 7, it is evident that the acoustic enclosure optimized using RSM exerts sound insulation effects on the fundamental frequency and second harmonic and third harmonic noise of the compressor, with the best performance observed for the fundamental frequency, achieving a reduction of 6.21 dB(A). After reinforcing the acoustic enclosure for rigidity, there is a noticeable enhancement in the sound insulation effectiveness. The rigidity-enhanced acoustic enclosure achieves a noise reduction of not less than 5 dB(A) for both the fundamental and harmonic frequencies, meeting expectations.

5. Conclusion

The low-frequency noise emitted by the air conditioner' compressor is primarily determined by the compressor's operating frequency and its lower harmonics. To mitigate the low-frequency noise issue in the compressor of a new indoor unit, this study has proposed a multilayered panel acoustic enclosure with enhanced rigidity. The conclusions drawn from the results are summarized as follows:

(1) The open area ratio and open area height are the primary factors influencing the actual sound insulation performance of the compressor' acoustic enclosure. Under fixed perforation conditions, the damping layer thickness ratio also affects the sound insulation performance. For the subject of this study, a damping layer thickness ratio of 0.1 proved to be the most suitable.

(2) Insufficient rigidity was identified as an issue in a thin-walled acoustic enclosure. The proposed "*X*"-shaped reinforcement measure effectively enhances the overall rigidity of the thin-walled acoustic enclosure. After rigidity enhancement, deformation of the acoustic enclosure decreases, resulting in reduced noise from vibration radiation.

(3) The optimized acoustic enclosure was manufactured for testing, and its effectiveness was evaluated in a semianechoic chamber. Experimental results indicate that the multilayered acoustic enclosure has a certain sound insulation effect, with the rigidity-optimized enclosure exhibiting superior performance.

(4) After installing the acoustic enclosure proposed in this study on the compressor, the fundamental frequency, second harmonic, and third harmonic noise of the compressor's operating frequency were reduced by 7.99 dB(A), 5.69 dB(A), and 5.19 dB(A), respectively. The acoustic enclosure can effectively isolate the compressor operation noise.

(5) Compared with traditional methods, the design optimization method of acoustic enclosure proposed in this paper is less dependent on the engineer's experience and experiment. The acoustic enclosure designed by this method is also verified to be effective by experiments. Future work will involve applying this type of acoustic enclosure to different air conditioning products.

Data Availability

All data used to support the findings of this study are included within the article, and there are no restrictions on data access.

Conflicts of Interest

The authors declare that they have no conflicts of interest.

Acknowledgments

The authors convey their thanks to the GD Midea Air-Conditioning Equipment Co., Ltd., for providing an experimental environment for this paper. This work was supported by the National Natural Science Foundation of China (Grant no. 52241101).

References

[1] M. Frontczak and P. Wargocki, "Literature survey on how different factors influence human comfort in indoor environments," *Building and Environment*, vol. 46, no. 4, pp. 922–937, 2011.

[2] Y. Chen, M. Li, J. F. Lu, and B. Chen, "Influence of residential indoor environment on quality of life in China," *Building and Environment*, vol. 232, 2023.

[3] Y. S. Choy, K. T. Lau, C. Wang, C. W. Chau, Y. Liu, and D. Hui, "Composite panels for reducing noise in air conditioning and ventilation systems," *Composites Part B: Engineering*, vol. 40, no. 4, pp. 259–266, 2009.

[4] J. Dandsena, K. Mohapatra, A. K. Satapathy, and D. P. Jena, "Noise control of outdoor unit of split type air-conditioner using periodic scatterers made with array of Helmholtz resonators," *Applied Acoustics*, vol. 179, 2021.

[5] Y. J. Mao, C. Fan, Z. P. Zhang, S. G. Song, and C. Xu, "Control of noise generated from centrifugal refrigeration compressor," *Mechanical Systems and Signal Processing*, vol. 152, 2021.

[6] C. J. Wu and X. F. Lei, "Noise control and sound quality evaluation of outdoor unit of split air-conditioner," *Journal of Measurements in Engineering*, vol. 4, no. 2, pp. 58–69, 2016.

[7] Y. Song, Q. Ma, T. Zhang, F. Li, and Y. Yu, "Research on vibration and noise characteristics of scroll compressor with condenser blockage fault based on signal demodulation," *International Journal of Refrigeration*, vol. 154, pp. 9–18, 2023.

[8] C. Wang, Z. Wang, W. G. Yan, H. K. Li, and C. L. Yang, "Study on characteristics of the vibration and noise of high-power scroll compressor," *Shock and Vibration*, vol. 2021, Article ID 5953133, 17 pages, 2021.

[9] M. Titze, M. Misol, and H. P. Monner, "Examination of the vibroacoustic behavior of a grid-stiffened panel with applied passive constrained layer damping," *Journal of Sound and Vibration*, vol. 453, pp. 174–187, 2019.

[10] X. Q. Zhou, D. Y. Yu, X. Y. Shao, S. Q. Zhang, and S. Wang, "Research and applications of viscoelastic vibration damping materials: a review," *Composite Structures*, vol. 136, pp. 460–480, 2016.

[11] F. Liu and J. Xu, "Nonlinear dynamic characteristics of High-entropy alloy-carbon fiber composite laminate subjected to stochastic excitation," *Materials Letters*, vol. 306, 2022.

[12] H. W. Wodtke and J. S. Lamancusa, "Sound power minimization of circular plates through damping layer placement," *Journal of Sound and Vibration*, vol. 215, no. 5, pp. 1145–1163, 1998.

[13] Z. Li and X. Liang, "Vibro-acoustic analysis and optimization of damping structure with Response Surface Method," *Materials & Design*, vol. 28, no. 7, pp. 1999–2007, 2007.

[14] T. L. Teng and N. K. Hu, "Analysis of damping characteristics for viscoelastic laminated beams," *Computer Methods in Applied Mechanics and Engineering*, vol. 190, no. 29-30, pp. 3881–3892, 2001.

[15] A. Fink and R. Schatz, "Structurally integrated constrained layer damping for noise reduction on sandwich and semi-monocoque helicopter structures," *Composite Structures*, vol. 322, 2023.

[16] V. Cool, O. Sigmund, N. Aage, F. Naets, and E. Deckers, "Vibroacoustic topology optimization for sound transmission minimization through sandwich structures," *Journal of Sound and Vibration*, vol. 568, 2024.

[17] X. Zhang and Z. Kang, "Topology optimization of damping layers for minimizing sound radiation of shell structures," *Journal of Sound and Vibration*, vol. 332, no. 10, pp. 2500–2519, 2013.

[18] F. Wu and P. Xue, "Dynamic topology optimization of constrained damping plates considering frequency and temperature characteristics based on an efficient strategy," *Shock and Vibration*, vol. 2024, Article ID 2155470, 19 pages, 2024.

[19] X. Wang, A. Zhang, F. Pang, and X. Yao, "Noise reduction analysis for a stiffened finite plate," *Journal of Sound and Vibration*, vol. 333, no. 1, pp. 228–245, 2014.

[20] Y. Y. Lee and C. F. Ng, "Sound insertion loss of stiffened enclosure plates using the finite element method and the classical approach," *Journal of Sound and Vibration*, vol. 217, no. 2, pp. 239–260, 1998.

[21] X. Cao, H. Hua, and Z. Zhang, "Sound radiation from shear deformable stiffened laminated plates," *Journal of Sound and Vibration*, vol. 330, no. 16, pp. 4047–4063, 2011.

[22] C. Shen, F. X. Xin, and T. J. Lu, "Sound transmission across composite laminate sandwiches: influence of orthogonal stiffeners and laminate layup," *Composite Structures*, vol. 143, pp. 310–316, 2016.

[23] G. Zhang, H. Zheng, and X. Zhu, "Optimization of composite plates with viscoelastic damping layer for high sound transmission loss under stiffness and strength constraints," *Composite Structures*, vol. 306, 2023.

[24] Q. Zhu, Q. Han, and J. Liu, "Topological optimization design on constrained layer damping treatment for vibration suppression of thin-walled structures via improved BESO method," *Aerospace Science and Technology*, vol. 142, 2023.

[25] G. Fusaro, S. D'Auria, and D. D'Orazio, "Multiphysical numerical analysis for acoustic metamaterials in ventilated ducts," *Inter-Noise and Noise-Con Congress and Conference Proceedings*, vol. 268, no. 4, pp. 4931–4942, 2023.

[26] Z. He, D. Li, Y. Han, M. Zhou, Z. Xing, and X. Wang, "Noise control of a twin-screw refrigeration compressor," *International Journal of Refrigeration*, vol. 124, pp. 30–42, 2021.

[27] M. Rim and Y. H. Kim, "Narrowband noise attenuation characteristics of in-duct acoustic screens," *Journal of Sound and Vibration*, vol. 234, no. 5, pp. 737–759, 2000.

[28] M. D. Rao, "Recent applications of viscoelastic damping for noise control in automobiles and commercial airplanes," *Journal of Sound and Vibration*, vol. 262, no. 3, pp. 457–474, 2003.

[29] M. Kliem, J. Høgsberg, J. Vanwalleghem et al., "Damping analysis of cylindrical composite structures with enhanced viscoelastic properties," *Applied Composite Materials*, vol. 26, no. 1, pp. 85–113, 2019.

[30] H. Chen, C. H. Lu, Z. Liu, C. R. Shen, Y. Sun, and M. L. Sun, "Structural modal analysis and optimization of SUV door based on response surface method," *Shock and Vibration*, vol. 2020, Article ID 9362434, 11 pages, 2020.

[31] S. Bhattacharya, "Central composite design for response surface methodology and its application in pharmacy," *Response Surface Methodology in Engineering Science*, 2021.

[32] H. Chang, S. Lu, Y. Sun, G. Zhang, and L. Rao, "Multi-objective optimization of liquid silica array lenses based on Latin hypercube sampling and constrained generative inverse design networks," *Polymers*, vol. 15, no. 3, p. 499, 2023.

[33] P. Wei, G. Yin, M. Shi, W. Zhang, and J. Feng, "Performance investigation and parameter optimization of ultra-light aerated concrete using orthogonal experimental design," *Case Studies in Construction Materials*, vol. 18, 2023.

[34] T. R. Sarker, S. Nanda, and A. K. Dalai, "Parametric studies on hydrothermal gasification of biomass pellets using Box-Behnken experimental design to produce fuel gas and hydrochar," *Journal of Cleaner Production*, vol. 388, 2023.

[35] Y. M. Tang, A. F. Zhou, and K. C. Hui, "Comparison of FEM and BEM for interactive object simulation," *Computer-Aided Design*, vol. 38, no. 8, pp. 874–886, 2006.
[36] J. Chen, Y. He, L. Gui, C. Wang, L. Chen, and Y. Li, "Aerodynamic noise prediction of a centrifugal fan considering the volute effect using IBEM," *Applied Acoustics*, vol. 132, pp. 182–190, 2018.
[37] E. Sundström, B. Semlitsch, and M. Mihăescu, "Acoustic signature of flow instabilities in radial compressors," *Journal of Sound and Vibration*, vol. 434, pp. 221–236, 2018.
[38] H. Y. Zhu, S. G. Lian, M. Jin et al., "Review of research on the influence of vibration and thermal fatigue crack of brake disc on rail vehicles," *Engineering Failure Analysis*, vol. 153, 2023.